Available online at www.sciencedirect.com
ScienceDirect
Proceedings of the Combustion Institute 33 (2011) 1245–1251
Proceedings of the Combustion Institute
www.elsevier.com/locate/proci

Multi-timescale modeling of ignition and flame regimes of *n*-heptane-air mixtures near spark assisted homogeneous charge compression ignition conditions

Yiguang Ju [a,*], Wenting Sun [a], Michael P. Burke [a], Xiaolong Gou [b], Zheng Chen [c]

[a] *Department of Mechanical and Aerospace Engineering, Princeton University, NJ 08544, USA*
[b] *School of Power Engineering, Chongqing University, Chongqing 400044, China*
[c] *SKLTCS, College of Engineering, Peking University, Beijing 100871, China*

Available online 18 October 2010

Abstract

The flame regimes of ignition and flame propagation as well as transitions between different flame regimes of *n*-heptane-air mixtures in a one-dimensional, cylindrical, spark assisted homogeneously charged compression ignition (HCCI) reactor are numerically modeled using a multi-timescale method with reduced kinetic mechanism. It is found that the initial mixture temperature and pressure have a dramatic impact on flame dynamics. Depending on the initial temperature gradient, there exist at least six different combustion regimes, an initial single flame front propagation regime, a coupled low temperature and high temperature double-flame regime, a decoupled low temperature and high temperature double-flame regime, a low temperature ignition regime, a single high temperature flame regime, and a hot ignition regime. The results show that the low temperature and high temperature flames have distinct kinetic and transport properties as well as flame speeds, and are strongly influenced by the low temperature chemistry. The pressure and heat release rates are affected by the appearance of different flame regimes and the transitions between them. Furthermore, it is found that the critical temperature gradient for ignition and acoustic wave coupling becomes singular at the negative temperature coefficient (NTC) region. The results show that both the NTC effect and the acoustic wave propagation in a closed reactor have a dramatic impact on the ignition front and acoustic interaction.

Keywords: HCCI; Flame dynamics; Low-temperature combustion; Ignition; Flame speed

1. Introduction

Recent concerns over energy sustainability calls for the need to develop advanced engine technologies to achieve improved energy conversion efficiency and reduced emissions [1,2]. These

* Corresponding author. Address: Department of Mechanical and Aerospace Engineering, Princeton University, Princeton, NJ 08544, USA.
E-mail address: yju@princeton.edu (Y. Ju).

1540-7489/$ - see front matter © 2010 The Combustion Institute. Published by Elsevier Inc. All rights reserved.
doi:10.1016/j.proci.2010.06.110

technologies include homogeneous charge compression ignition (HCCI) [3–5] and spark assisted HCCI (SAHCCI) [6,7] engines as well as low-temperature combustion (LTC) engines [8–11]. Unfortunately, the difficulties in combustion and emission control in these advanced engines remain a major challenge. At temperatures below 1500 K, increased CO emissions reduce the engine efficiency. On the other hand, for temperatures above 1800 K, HCCI engines are limited by NO_x emissions and knocking [12]. Therefore, the control of combustion processes such as ignition and flame propagation is critical for efficient engine development. To achieve this goal, the SAHCCI as well as thermal and concentration stratification techniques [13,14] have been developed. However, the combustion process of SAHCCI engines are strongly influenced by the complexity of low temperature chemistry and the variation of transport properties, particularly near the negative temperature coefficient (NTC) region. In addition, many practical engine fuels exhibit two-stage ignition phenomena [15,16]. Therefore, understanding of unsteady combustion regimes at near HCCI conditions involving the NTC chemistry, transport process, and acoustic wave compression is important.

A number of studies have been conducted to understand ignition and flame propagation in HCCI/SAHCCI combustion using experiments [7,17] and analyses with simplified models [18–21]. Different combustion regimes such as spontaneous ignition, flame deflagration, and detonation have been observed. The criteria for the occurrence of these combustion regimes have been studied using hydrogen/air mixtures or global kinetic models [22–26]. The results show that the initial temperature and species gradients play an important role in affecting flame regimes. Unfortunately, few studies have been conducted to understand the mechanism of flame transition involving large hydrocarbon fuels. Moreover, the two-stage low temperature ignition (LTI) and hot ignition regimes at NTC region play a dominant role in affecting the flame regimes and transition to auto-ignition. However, due to the complexity of large chemical kinetic mechanisms for large hydrocarbon fuels, the flame dynamics near the NTC region at SAHCCI/HCCI conditions has not been well understood. Recently, in order to understand the flame transition from deflagration to auto-ignition, Martz et al. [21] used a separated ignition and flame propagation model coupled with SENKIN and PREMIX codes [27,28] and a skeletal iso-octane mechanism. It was concluded that transport had little effect on reaction front propagation when ignition had occurred. Unfortunately, due to the limitation of the use of the separated ignition and flame propagation model, the transport effect of initial ignition kernel and the acoustic wave couplings with flame front evolution and chemical kinetics were not considered. More importantly, the use of a skeletal iso-octane mechanism may exclude the observation of important combustion regimes caused by the low temperature chemistry.

The goal of this paper is to simulate the different regimes of ignition, flame propagation, and detonation transition of combustion at HCCI and SAHCCI conditions of *n*-heptane-air mixtures by using a one-dimensional, cylindrical SAHCCI reactor and a multi-timescale (MTS) method with a reduced kinetic mechanism generated automatically by the path flux analysis method.

2. Numerical models

To model SAHCCI and HCCI combustion, we consider simplified, unsteady flame kernel propagation in a one-dimensional (1D), non-adiabatic closed cylinder (Fig. 1). Although turbulence is important in HCCI combustion, we limit our focus to understand laminar combustion regimes. The SAHCCI reactor height is 8 mm with a radius of 4 cm. All the wall temperatures are fixed at 500 K. Both the top and bottom surfaces of the reactor are subject to convective heat losses with a constant Nusselt number (*Nu*) of 4.36 [29]. Symmetric boundary conditions are assumed at the centerline of the reactor. To model the effects of low temperature chemistry on combustion regimes, we use *n*-heptane as the fuel. A detailed kinetic model for *n*-heptane with 1034 species [30,31] is used. The path flux analysis method [32] is used to generate a reduced mechanism with 128 species and 565 elementary reactions. As shown in Fig. 2a, the reduced mechanism with 128 species is sufficiently comprehensive to reproduce both the ignition delay time at the NTC region. The governing equations of the one-dimensional, unsteady, compressible, multi-component, reactive flow are modeled by using the ASURF code developed at Princeton University [33]. The code was extensively tested for ignition time and flame speeds of hydrogen, methane, propane, and *n*-heptane/air mixtures using CHEMKIN-II package [28]. The MUSCL-Hancock scheme [34] is adopted to enable shock capturing capability. The detailed transport and kinetic models are computed using the hybrid multi-timescale (HMTS) method [35]. Unless otherwise stated, the initial pressure and equivalence ratio are 20 atm and 0.4, respectively. Unless otherwise stated, the initial temperature distribution is uniform and varied between 600 and 1100 K. To initiate flame propagation, a hot kernel of 1400 K with a radius of 1 mm was initially created at the centerline of the SAHCCI reactor. The grid size is adapted at each time step with a minimum grid size of 10 μm located at the flame

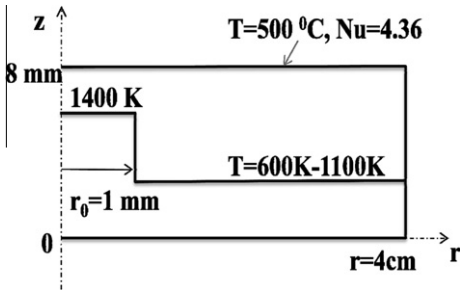

Fig. 1. Schematic of the one-dimensional cylindrical SAHCCI/HCCI reactor.

front. The grid size effect on the flame trajectory and laminar flame speed are tested for stoichiometric *n*-heptane/air mixture at atmospheric pressure with the minimum grid sizes of 16 and 4 μm, respectively. The difference in flame front trajectory is found to be negligible.

3. Results and discussion

3.1. Effects of initial temperature on flame regimes and transition to ignition

Figure 2b shows the dependence of ignition delay time on temperature of *n*-heptane-air mixtures at equivalence ratio of 0.4. It is seen that with the increase of pressure, the NTC region shifts to higher temperatures. At 20 atm, the NTC region is between 850 and 940 K.

Figure 3 shows the pressure histories at the centerline of the SAHCCI reactor for temperatures at 1000, 700, and 600 K. At 1000 K, which is above the NTC temperature (Fig. 2b), hot ignition occurs at 5 ms and causes strong acoustic wave oscillations in the reactor. However, at

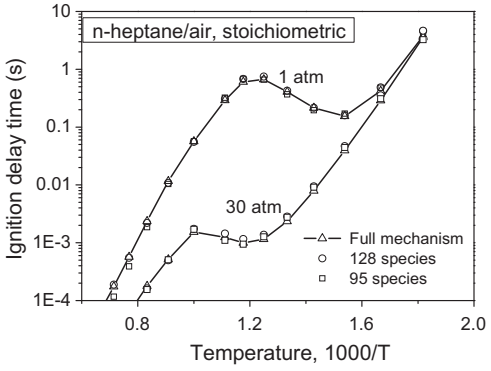

Fig. 2a. Comparisons of predicted ignition delay time using full and reduced mechanisms (95 and 128 species) generated by path flux analysis for stoichiometric *n*-heptane-air mixtures at 1 and 30 atm, respectively.

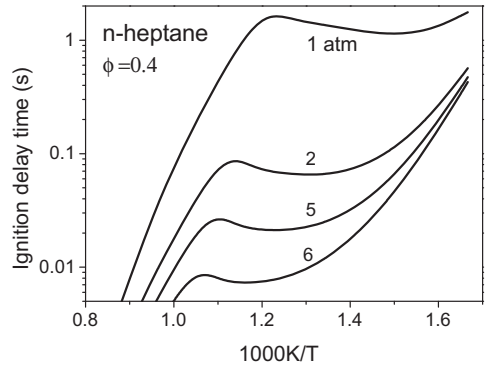

Fig. 2b. Dependence of ignition delay time of *n*-heptane-air mixtures at equivalence ratio of 0.4 on the initial temperature.

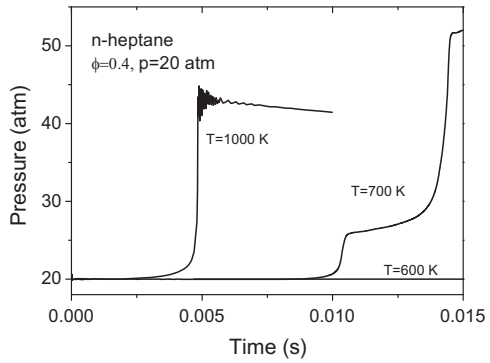

Fig. 3. The transient pressure histories at the centerline of the SAHCCI reactor of *n*-heptane-air mixtures at equivalence ratio of 0.4 for initial temperatures at 1000, 700, and 600 K, respectively.

700 K, Fig. 3 shows that there is a two-stage pressure rise at 10 and 14 ms, respectively. At 600 K, the auto-ignition delay time is very long and the pressure in the reactor does not change noticeably within 40 ms.

The evolution histories of the flame front (defined as the location of the maximum chemical heat release rate) for initial temperatures of 1000, 600, and 700 K in the 1D SAHCCI reactor are plotted in Figs. 4a and 4b. In Fig. 4a, it is seen that at 1000 K, a quasi-steady-state flame propagates at the speed of 1 m/s before the occurrence of the hot ignition at 5 ms. For temperature at 600 K, the combustion is dominated by laminar flame propagation. The laminar flame speed is about 5.4 cm/s. The large flame speed difference originates from the change of the high temperature flame (HTF) at 1000 K and the low temperature flame (LTF) at 600 K. Here, the HTF and LTF are, respectively, governed by the high temperature and low temperature kinetic mechanisms with different species concentrations.

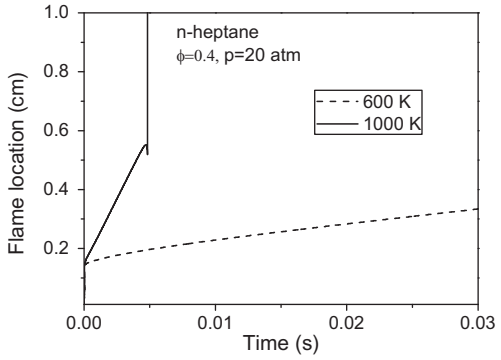

Fig. 4a. Transient history of flame fronts at the maximum heat release rate in the SAHCCI reactor at $T = 1000$ and 600 K, respectively.

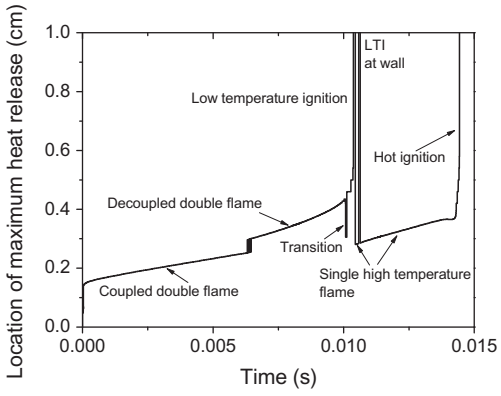

Fig. 4b. Transient history of flame fronts at the maximum heat release rate in the SAHCCI reactor at $T =$ K.

However, at 700 K, Fig. 4b shows a completely different flame trajectory. After the initial flame kernel evolution, there exist two different flame structures, the HTF and the LTF. Before $t = 6.3$ ms, the HTF and LTF are coupled and the coupled flame structure propagates at a speed of 15.3 cm/s. At 6.3 ms, the LTF starts to decouple from the HTF and propagates at a much faster flame speed (27.5 cm/s) than the HTF. In this case, the species concentrations in from of the LTF have changed dramatically due to the progress of the low temperature reactions. As the low temperature ignition chemistry proceeds further, the LTF propagation speed increases with time – indicating a strong coupling between ignition and flame propagation. At time around 10 ms, the low temperature ignition (LTI) occurs. After LTI is completed at 10.5 ms, the LTF disappears and leads to a single HTF propagation regime. The single HTF propagates at a speed around 25.6 cm/s until the hot ignition occurs at 14 ms. Therefore, at near NTC region, there exist many different flame regimes; their burning rates and their transitions to ignition are dependent on the transport properties and detailed chemical kinetics.

3.2. Effects of initial temperature and chemical kinetics on flame structures

To examine the flame structures of the LTF and HTF, Fig. 5a and b show the distribution of heat release rates of the six different flame regimes for initial temperature of 700 K. Figure 5a shows that the early ignition initiated by the hot spot (1400 K) in the center of the reactor results in a single flame kernel propagation at 0.1 ms. However, at 3.0 ms, the single reaction zone splits into two reaction zones, a weak LTF zone and a strong HTF. This is the coupled double-flame structure shown in Fig. 4b. At 9.3 ms, the LTF and HTF decouple and the LTF becomes stronger and propagates faster than HTF. At 10.35 ms, Fig. 5b shows that the LTI occurs in front of the LTF. This is the transition from the LTF to the low temperature ignition regime. As a result, the strength of the LTF decreases as the LTI proceeds. At 12.70 ms, the LTI ends and the LTF disappears. Therefore, there is only one HTF front located at $r = 0.35$ cm. At 14.30 ms, Fig. 5b shows that the hot ignition in front of the HTF develops and leads to the transition to the hot ignition regime.

The corresponding temperature distributions of Fig. 5 are shown in Fig. 6. Figure 6a shows clearly that at the coupled LTF and HTF regime before 6.3 ms, there is only one temperature front. However, at the decoupled double-flame regime between 6.3 and 10 ms, the temperature distribution shows that there are two distinct flame fronts and each flame front has a different flame propagating speed. The different flame speeds between LTF and HTF originate from the differences in their activation energies and transport properties. At 10.35 ms, LTI occurs and results in a propagating HTF before the hot ignition starting at 14.80 ms.

The structure of the decoupled double-flame regime in Figs. 4a,b and 5 at $t = 9.3$ ms for initial temperature of 700 K is plotted in Fig. 7. Figure 7a shows that at the LTF front ($x = 0.4$ cm), *n*-heptane decomposes completely and leads to the rapid increase of HO_2 and H_2O_2. On the other hand, at the HTF front, the concentrations of HO_2, H_2O_2, and CO decrease, resulting in rapid formation of H_2O and CO_2. Therefore, we can use the production and destruction of H_2O_2 as a criterion to distinguish the onsets of low temperature flame and high temperature flame, respectively. Figure 7b shows the typical intermediate hydrocarbon species in the LTF zone. It is observed that a large amount of aldehydes (CH_2O, CH_3CHO, and C_2H_5CHO) are formed at the LTF zone. In addition, flux analysis shows that small olefins (C_2H_4, C_3H_6) are formed from the decomposition of the alkyl radicals,

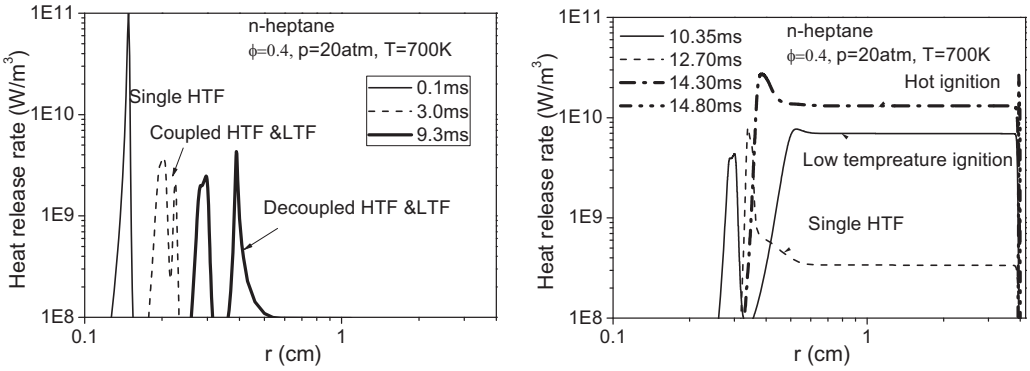

Fig. 5. a (left) and b (right): transient distributions of chemical heat release rates at $T = 700$ K.

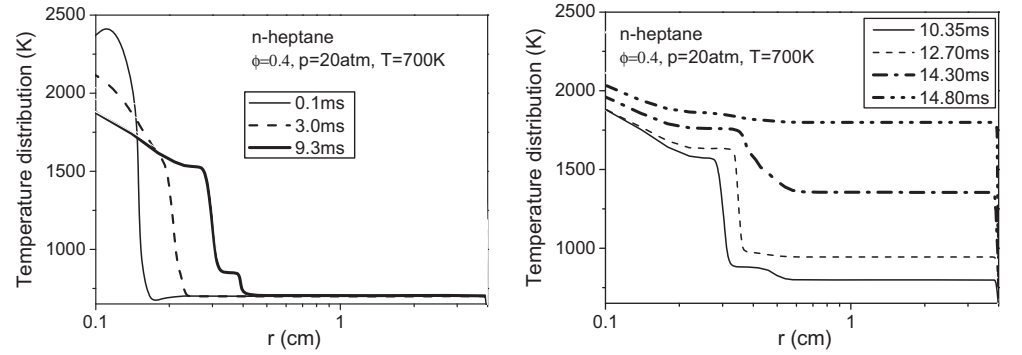

Fig. 6. a (left) and b (right): transient distributions of temperature at $T = 700$ K.

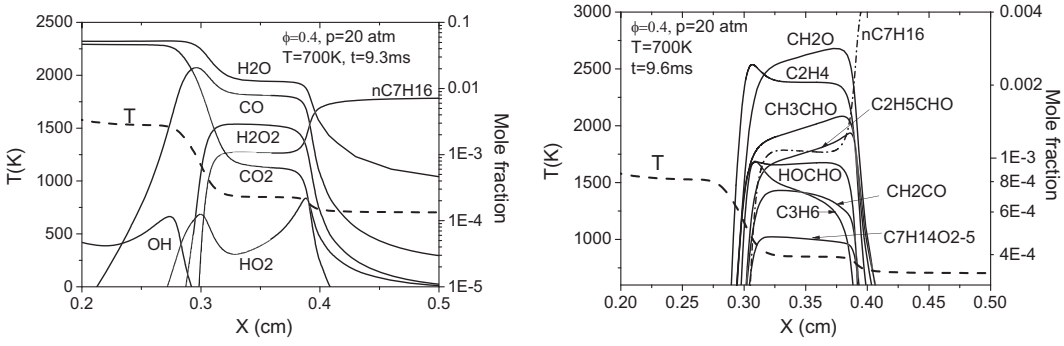

Fig. 7. a (left) and b (right): distributions of temperature and species of the decoupled double-flame regime at 9.3 ms for $T = 700$ K.

$C_7H_{14}O_2$-5 and nC_7ket24 after isomerization and decomposition of $C_7H_{14}OOH$ and $O_2C_7H_{14}OOH$ [15]. Since the flame propagation is affected by the fuel chemistry and the transport of major species, the dual flame structure shows that the oxidation and transport properties of olefins and aldehydes formed in the LTF will affect dramatically the HTF flame chemistry and speed and makes completely different from that of LTF. As such, both the low temperature chemistry and the transport affect significantly the flame regimes and heat release rates of SAHCCI combustion.

3.3. Diagram of critical temperature gradient for flame front and acoustic wave coupling

In practical SAHCCI and HCCI engines, the temperature distribution is not always uniform.

Therefore, the chemical kinetics will not only contribute to the formation of new flame regimes but also affects the coupling between ignition/flame fronts and acoustic waves. For simple fuels such as hydrogen without low temperature chemistry, the critical temperature gradient at which the auto-ignition front speed becomes equal to the sonic speed of the unburned mixture decreases monotonically with the decrease of temperature [22,23]. However, the existence of the NTC region for the gasoline and diesel fuels will make the temperature dependence of the critical temperature gradient completely different. Figure 8 shows the critical temperature gradient dependence on the initial mixture temperature. The critical temperature gradient is calculated by equating the acoustic speed of the mixture to the propagation speed (a) of the ignition front,

$$a = \left(\left.\frac{\partial T}{\partial r}\right|_c \times \frac{\partial \tau_{ig}}{\partial T}\right)^{-1} \quad (1)$$

The temperature gradient of ignition delay time and the acoustic speed are evaluated by using CHEMKIN [27]. Unlike that at high and low temperature regions, the critical temperature gradient becomes singular (negative and positive infinities) at the NTC region. This is caused by the negative temperature dependence of the ignition delay time on temperature in the NTC region. The appearance of infinite critical temperature gradient for ignition front and acoustic wave coupling reveals that the NTC effect promotes supersonic auto-ignition and decouples ignition front and acoustic wave coupling at low temperature gradients. Figure 9 shows the time history of ignition flame front with an initial temperature gradient of 400 K/m (linear temperature distribution from 866 to 850 K in the radial direction) in the reactor. The small noise near 4 ms is due to the sensitivity of the location of the maximum heat release rate to kinetic mechanism in a uniformly distributed mixture. Although this

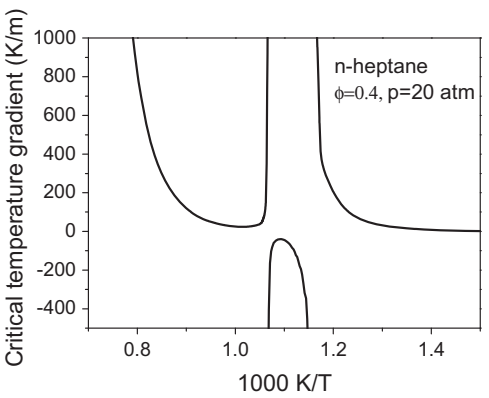

Fig. 8. The effect of NTC chemistry on the singular dependence of the critical temperature gradient on temperature.

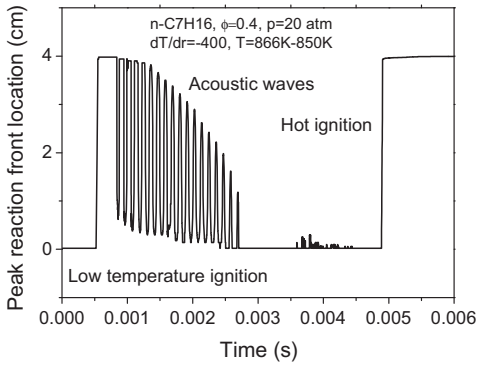

Fig. 9. The reaction front with the maximum heat release with an initial temperature gradient of 400 K/m (866–850 K in the radial direction).

temperature gradient is much greater than the critical temperature gradients before and after the NTC regions (Fig. 8), Figure 9 shows that in the NTC region no ignition to detonation transition is observed. Instead, only supersonic low temperature ignition front ($t = 0.5$ ms) and high temperature ignition front ($t = 4.9$ ms) are observed. In addition, both the low temperature ignition and the acoustic wave propagation (the front oscillation in Fig. 9) in the closed reactor reduce the initial temperature gradient. As a result, the occurrence of spontaneous ignition is promoted and the transition to detonation is suppressed.

4. Conclusion

The ignition, flame propagation, and ignition front and acoustic wave coupling of *n*-heptane-air mixtures in a one-dimensional, cylindrical SAHCCI reactor are numerically modeled at NTC conditions using a multi-timescale method. It is found that at near NTC temperatures, there are six different combustion regimes, an initial single flame front propagation regime, a coupled LTF and HTF double-flame regime, a decoupled LTF and HTF double-flame regime, a low temperature ignition regime, a single HTF regime, and a hot ignition regime. Both the transport and low temperature chemical kinetics affect the flame regimes, flame to ignition transition, pressure history, and chemical heat release rates. It is also found that the critical temperature gradient for ignition front coupling with acoustic waves become singular at the NTC region. The NTC effect promotes the formation of supersonic auto-ignition and decouples the acoustic wave-ignition front coupling at low temperature gradients.

Acknowledgments

This research is jointly supported by the Air Force Office of Scientific Research (AFOSR)

MURI research program under the guidance of Dr. Julian Tishkoff and the US Department of Energy, Office of Basic Energy Sciences as part of an Energy Frontier Research Center on Combustion with Grant No. DE-SC0001198. Y.J. thank Steve Dooley at PU for many helpful discussions on chemistry.

Appendix A. Supplementary data

Supplementary data associated with this article can be found, in the online version, at doi:10.1016/j.proci.2010.06.110.

References

[1] DOE Basic Energy Sciences Workshop, Basic Energy Needs for Clean and Efficient Combustion of 21st Century Transportation Fuels. 2007. Available at http://www.science.doe.gov/bes/reports/files/CTF_rpt.pdf.
[2] M. Colket, T. Edwards, S. Williams, et al., *AIAA-Paper* 2007-770, 2007.
[3] J.E. Dec, *Proc. Combust. Inst.* 32 (2) (2008) 2727–2742.
[4] M. Noguchi, Y. Tanaka, T. Tanaka, Y. Takeuchi, *SAE Technical Paper Series*, Paper No. 790840, 1979.
[5] M. Christensen, B. Johansson, *SAE Trans.* 107 (4) (1998) 951–963, Paper 982454.
[6] H. Kopecek, E. Winter, M. Lackner, F. Winter, A. Hultqvist, *SAE Technical Paper Series*, Paper No. 2004-01-0937, 2004.
[7] H. Persson, A. Hultqvist, B. Johansson, A. Remon, *SAE Technical Paper Series*, Paper No. 2007-01-0212, 2007.
[8] M. Christensen, A. Hultqvist, B. Johansson, *SAE Trans.* 108 (3) (1999), Paper 1999-01-3679.
[9] Y. Iwabuchi, K. Kawai, T. Shoji, Y. Takeda, *SAE Trans.* 108 (3) (1999), Paper 1999-01-0185.
[10] J.E. Dec, R.E. Canaan, *SAE Trans.* 107 (3) (1998) 176–204, Paper 980147.
[11] N. Kaneko, H. Ando, H. Ogawa, N. Miyamoto, *SAE Trans.* 111 (3) (2002) 2309–2315, Paper 2002-01-1743.
[12] T. Tsurushima, *Proc. Combust. Inst.* 32 (2009) 2835–2841.
[13] M. Sjoberg, J.E. Dec, N. Cernansky, *SAE Technical Paper Series*, Paper No. 2005-01-0113, 2005.
[14] W. Hwang, J.E. Dec, M. Sjoberg, *SAE Technical Paper Series*, Paper No. 2007-01-4130, 2007.
[15] H.J. Curran, P. Gaffuri, W.J. Pitz, C.K. Westbrook, *Combust. Flame* 114 (1998) 149–177.
[16] K. Kuma, C.-J. Sun, *Fuel Summit*, University of Southern California, Los Angeles, CA, September 17, 2009.
[17] A. Hultqvist, M. Christensen, B. Johansson, et al. *SAE Technical Paper Series*, Paper No. 2002-01-0424, 2002.
[18] R.A. Cox, J.A. Cole, *Combust. Flame* 60 (1985) 109.
[19] M. Schreiber, Sadat A. Sakak, A. Lingens, J.F. Griffiths, *Proc. Combust. Inst.* 25 (1994) 933–940.
[20] J.S. Cowert, J.C. Keck, J.B. Heywood, *Proc. Combust. Inst.* 23 (1990) 1055–1062.
[21] J.B. Martz, H. Kwak, H.G. Im, G.A. Lavoie, D.N. Assanis, S.B. Fiveland, Propagation of a reacting front in an auto-igniting mixture, in: *Proceedings of the Sixth US National Combustion Meeting*, Michigan, 2009.
[22] D. Bradley, X.J. Gu, D.R. Emerson, *Combust. Flame* 133 (2003) 63–74.
[23] Y. Zeldovich, *Combust. Flame* 39 (1980) 211–214.
[24] R. Sankaran, H. Im, E. Hawkes, J. Chen, *Proc. Combust. Inst.* 30 (2005) 875–882.
[25] J.H. Chen, E.R. Hawkes, R. Sankaran, S.D. Mason, H.G. Im, *Combust. Flame* 145 (2006) 128–144.
[26] E.R. Hawkes, R. Sankaran, P. Pebay, J.H. Chen, *Combust. Flame* 145 (2006) 145–159.
[27] A. Lutz, R. Kee, J. Miller, Sandia National Laboratory Report SAND87-8248, 1988.
[28] R. Kee, J. Grcar, M. Smooke, J. Miller, *A Fortran Program for Modeling a Steady Laminar One-Dimensional Premixed Flame*, Technical Report SAND85-8240, Sandia National Laboratories, 1985.
[29] J.P. Holman, *Heat Transfer*, ninth ed., McGraw Hill Inc., 2002, pp. 245–248.
[30] H.J. Curran, P. Gaffuri, W.J. Pitz, C.K. Westbrook, *Combust. Flame* 129 (2002) 253–280.
[31] Available at http://www-cmls.llnl.gov/data/docs/science_and_technology/chemistry/combustion/nc7_2b_mech.txt.
[32] Wenting Sun, Zheng Chen, Xiaolong Gou, Yiguang Ju, *Combust. Flame* 157 (2010) 1298–1307.
[33] Zheng Chen, Michael P. Burke, Yiguang Ju, *Proc. Combust. Inst.* 32 (2009) 1253–1260.
[34] B. van Leer, *SIAM J. Sci. Stat. Comput.* 5 (1984) 1–20.
[35] X. Gou, W. Sun, Z. Chen, Y. Ju, *Combust. Flame* 157 (2010) 1111–1121.